Calibration of 2D Camera and 3D Sensor for Non-Contact Metrology Applications

Somayeh Hesabi[1] and Denis Laurendeau[1]
[1]*Computer Vision and Systems Laboratory, Laval University , Québec, Canada*
somayeh.hesabi.1@ulaval.ca, denis.laurendeau@gel.ulaval.ca

Keywords: Calibration, Metrology, Inspection, Non-Destructive Testing, 3D Modeling.

Abstract: Laser scanning and stereo vision systems have enabled researchers to design and implement 3D object modeling approaches. Moreover, Non-Destructive Testing (NDT) makes it possible to inspect subsurface defects of objects without changing or destroying their functionality. In this paper, we propose a reliable and repeatable calibration approach to combine the 3D data of elongated structures acquired by handheld 3D scanners and infrared information provided by IR cameras. The results indicate that the calibration procedure is applicable to metrology applications on very long structures. Pipelines are chosen as typical instances of such elongated structures.

1 INTRODUCTION

Although pipelines play an important role in the energy infrastructure in order to transport liquid or natural gas safely, they are vulnerable to external and internal damages. Accordingly, a periodic inspection of pipelines is crucial to increase their functionality and decrease the environmental disasters as well as economic losses caused by potential spills, explosions or other malfunctions.

Considering the benefits of 3D sensors which allow us to create an accurate digital replica of the surface of physical objects in addition to the advantages of Non-Destructive Testing (NDT) technology which provides the ability of under-surface monitoring, our research proposes a solution to build a 3D model of pipeline or other elongated structures to monitor their status.

As the 3D scanner and IR sensor acquire the information in their own local reference frames, we need to define very accurately the relationship between these coordinate systems to be able to combine them. In this paper, we propose an accurate and repeatable approach for calibrating a 2D camera and 3D sensor. The metrology aspect of the approach is thus the focus of this paper.

For the purpose of illustrating the different calibration steps and mapping operation more visually, the IR camera is replaced by an standard color 2D visible camera. Using a visible camera with higher resolution compared to the IR sensor enables us to estimate and visualize the level of accuracy of the proposed calibration procedure for qualitative assessment of mapping results. The rest of the paper is organized as follows: Section 2 details related works. The proposed calibration approach is explained in Section 3. In Section 4 and 5 the experimental results and conclusions are presented.

2 RELATED WORK

Despite the recent advances in robotics and computer vision applications, 2D camera-3D range sensor calibration is still a challenging problem in multi-sensor frameworks in order to represent the information in a common coordinate system. Assuming a valid intrinsic calibration of the 2D camera, the estimation of the rigid transformation between this camera and the range sensor is required in order to align their local coordinate frames. In general, the extrinsic multi-sensor calibration techniques can be classified into two groups: approaches that use known calibration targets like fiducial markers or planar checkerboards (Wasielewski and Strauss, 1995; Unnikrishnan and Hebert, 2005), and targetless calibration methods (Scaramuzza et al., 2007; Levinson and Thrun, 2013; Pandey et al., 2015). In the first group, the calibration target should be located in the field of view of both sensors while, in the second group, the calibration parameters are computed based on corresponding features found in natural scenes consid-

(a) (b)

Figure 1: The 3D scanner and the photogrammetric tracker. (a) Creaform MetraSCAN handheld 3D scanner with retro-reflective markers tracked by the C-Track. (b) Creaform C-Track photogrammetric tracker.

ering the perspective-from-n-points (PnP) algorithm (Quan and Lan, 1999). Even though targetless approaches are independent of a known calibration target, the natural scenes can lead to an unreliable calibration or may completely fail in some instances (Levinson and Thrun, 2013; Napier et al., 2013). Although these methods can provide a good estimation of the calibration parameters, they are generally applicable in environment perception, path planning and mapping, navigation and mobile robotics in which the accuracy and repeatability are not as crucial as they are for metrology applications. In this paper, we propose a reliable and highly repeatable calibration procedure which is applicable to metrology applications on very long structures. Contrary to the above mentioned approaches that use 3D/2D LiDAR, radar or sonars as range sensors, we use the high precision Creaform MetraSCAN metrology handheld scanner that is tracked by Creaform C-Track780 photogrammetric system (see figure 1). The C-Track dual-camera sensor (with 7.8 m^3 measuring volume) is able to measure the reflectors within its operating space and track the MetraSCAN optical CMM scanner. The MetraSCAN scanner acquires the 3D measurements using a laser-cross with an accuracy of up to 86 µm. Moreover, the portability of Creaform scanners enables us to capture the data from the surface of pipelines, so there is no need to filter out the object of interest from the rest of the scene which is the case for the above mentioned sensors.

3 Proposed Approach

In this work, the non-inverting pinhole camera model is adopted. Calibrating a single-camera is the procedure of estimating the parameters of the camera model which describe the geometric relationship between a pixel in an image and its corresponding point in 3D space. Calibration parameters consist in two sets: intrinsic and extrinsic parameters (Ouellet, 2011).

3.1 Intrinsic Calibration

The intrinsic parameters are specific to the camera and independent of its pose in the scene. They give the relationship between an image point $\mathbf{p} = [u, v, 1]^T$ in pixel coordinates and its coordinates in the sensor reference frame $\mathbf{x} = [x, y, 1]^T$.

The intrinsic parameters of the pinhole model can be modeled by a 3×3 matrix $\mathbf{K}$:

$$\mathbf{K} = \begin{bmatrix} f_u & 0 & u_0 \\ 0 & f_v & v_0 \\ 0 & 0 & 1 \end{bmatrix}, \ \mathbf{p} = \mathbf{K}\mathbf{x}, \tag{1}$$

where f_u and f_v are the focal lengths in the horizontal and vertical axes of the image, respectively and $[u_0, v_0]$ are the coordinates of the principal point (see figure 2).

In addition to the above, four other intrinsic parameters, k_1 and k_2, model the radial distortion and p_1 and p_2 model the tangential distortion and are used to take into account the effect of the lens on the image formation process implemented by the pinhole.

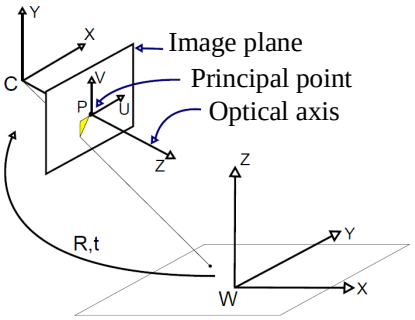

Figure 2: Camera pinhole model (figure taken from (Ouellet, 2011)). Projection model: the principal point P is the intersection of the optical axis with the image plane. The camera pose consists in a rotation and translation $(\mathbf{R}, \mathbf{t})$ which transforms a 3D point in the target reference frame $\mathbf{W}$ into the camera reference frame $\mathbf{C}$.

3.2 Extrinsic Calibration

The camera pose in the scene is represented by extrinsic parameters which is a rigid transformation consisting in a rotation and a translation. It transforms the points in the global reference frame of the calibration target into the local reference frame of the camera (see figure 2). The combination of intrinsic and extrinsic parameters provides the relationship between a 3D point in the target reference frame and its projection on the image plane according to the following perspective projection model. The camera pose in the scene is represented by extrinsic parameters which is a rigid transformation consisting in a rotation and a translation. It transforms the points in the global reference frame of the calibration target into the local reference frame of the camera (see figure 2). The combination of intrinsic and extrinsic parameters provides the relationship between a 3D point $\mathbf{X}$ in the target reference frame and its projection on the image plane according to the following perspective projection model:

$$\lambda \begin{bmatrix} u \\ v \\ 1 \end{bmatrix} = \mathbf{K} \begin{bmatrix} \mathbf{R} \mid \mathbf{t} \end{bmatrix} \begin{bmatrix} X \\ Y \\ Z \\ 1 \end{bmatrix} = \mathbf{PX}, \qquad (2)$$

where $\mathbf{R}_{3\times3} \in SO(3)$ and $\mathbf{t}_{3\times1}$ are the rotation and translation matrices, respectively. Matrix $\mathbf{P}_{3\times4}$ is called the camera matrix.
Theoretically, a set of six correspondences between the image and the target which are uniformly distributed within the volume of the scene are enough for the estimation of matrix $\mathbf{P}$. In practice, we use more than six correspondences to increase the robustness of the estimation and reduce the effect of noise (Ouellet, 2011).

We use a 2D planar target with $16 \times 16 = 256$ circular markers to calibrate the intrinsic parameters as illustrated in figure 3. The superiority of circular markers over checkerboard and butterfly-type markers has been recently investigated in (Ouellet, 2011).

3.2.1 Tracking the 2D Camera Using the Photogrammetric Sensor

Installing retro-reflective markers on the 2D camera that are visible from the photogrammetric tracker enables us to track this camera and define the transformation between the camera case and the coordinate frame of the tracker as mentioned previously. The photogrammetric tracker computes the 3D coordinates of the markers in its reference frame. The configuration of markers (called the tracking model in the following) has a significant effect on the tracking accuracy and mapping as well. Considering the relevant literature (Woltring et al., 1985), the following constraints must be considered before designing a tracking model:

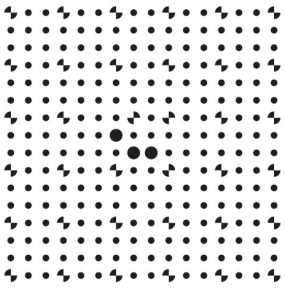

Figure 3: Precise metrologic calibration target made of multiple chrome markers engraved in an opal glass plate.

1) The best accuracy is achieved when the markers are distributed on a sphere with equal distance around the point of interest [1]. In our case the focus of interest is the pose of the tracking model. However, we have to make sure that the tracking model can be used in practice (West and Maurer, 2004).
2) Increasing the number of markers obviously improves the accuracy although the probability of occlusion increases as well (Fitzpatrick et al., 1998).
3) Propagated rotational errors have the most significant impact on the final tracking error which has the smallest value at the centroid of markers. Although it is not always possible to position markers in a way that the centroid lies at the point of interest, we can make sure that the points are as close as possible to the centroid of the markers. By close, we mean close relative to the radius of markers' distribution (Woltring et al., 1985).
4) A wider distribution of the markers in space increases the rotational accuracy as long as the tracking model is usable (Woltring et al., 1985; Fitzpatrick et al., 1998).
5) Increasing the size of markers on the image plane by using larger markers, increasing the resolution of the camera chip, or using a greater focal length as well as changes in the lighting conditions or the detection algorithms. However, we could not consider this constraint as we use a commercial tracking system (the Creaform C-Track) that is

[1] In some applications, instead of using the pose of the tracking model directly, some point of interest defined in the coordinate frame of the target is used, such as the tip of a probe (Bauer et al., 2006).

designed to work in various environmental conditions.

6) Non-coplanar targets significantly improve the accuracy of rotational and distance estimations compared to coplanar targets (Vogt et al., 2002).

According to the aforementioned constraints and C-Track's specifications, we built the tracking model presented in figure 4. The non-coplanar target includes a planar plate with posts of different lengths to improve the accuracy of 3D tracking. Planar circular retro-reflective markers are installed on the plate and at the tip of each post.

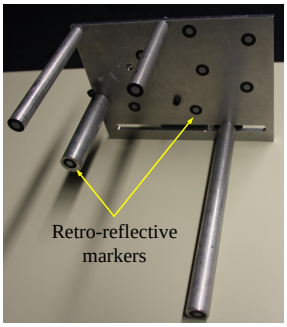

Figure 4: The non-coplanar target model.

In addition to the markers' configuration, the accuracy of pose estimation can be improved by removing the outliers as the data provided by the tracker is noisy. We use the absolute deviation around the median (MAD) as a robust criterion to remove the outliers (Leys et al., 2013). Let us assume that $\mathbf{X} = \{x_1, x_2, ..., x_i\}$ is the set of original observations and m_X is the median of set $\mathbf{X}$. MAD is defined as the median of set $\mathbf{Y} = \{|x_1 - m_X|, |x_2 - m_X|, ..., |x_i - m_X|\}$. Then, the data point x_i is an inlier if:

$$|x_i - m_X| < 2.5\ \mathbf{MAD}. \quad (3)$$

Then, we apply an ICP refinement (Besl and McKay, 1992) on the filtered data points in order to align them to the physical target model to increase the accuracy of estimating pose of markers.

3.2.2 Tracker-Camera Calibration

Looking at figure 5, the transformation matrix $\mathbf{M}$ from the markers (attached to the camera case) to the camera coordinate system is unknown. The problem of determining this relationship (called the *calibration matrix* in the following) is referred to as the tracker-camera calibration problem. One can estimate this relationship by defining a precise target with a known geometry in 3D space which is visible in both coordinate frames and closes the loop $\mathbf{AMB} = \mathbf{C}$. Matrices $\mathbf{A}$, $\mathbf{B}$ and $\mathbf{C}$ are the markers' transformation from tracker, the extrinsic parameters of camera with respect to the target and the target's transformation from the tracker, respectively.

It should be mentioned that a major goal of this paper is to propose a precise procedure for projecting the information contained in the image of the 2D (or IR) camera on the surface of extended structures scanned using the 3D scanner. The accuracy of this projection is highly dependent on the accuracy of the estimation of the calibration matrix $\mathbf{M}$. Hence, we use a three dimensional target (as presented in figure 6) which is ideal for achieving the best possible accuracy. Using this target we obtained a sub-millimeter accuracy of projection based on the estimated calibration matrix $\mathbf{M}$. The details of the calibration procedure are presented in the following.

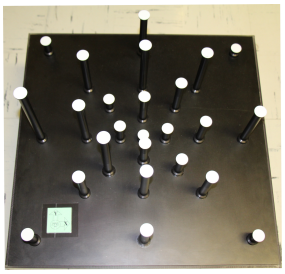

(a)

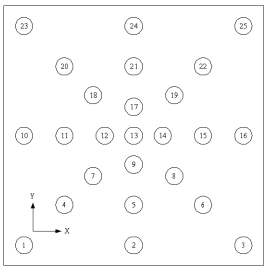

(b)

Figure 6: (a) A picture of the 3D target used to find the calibration matrix $\mathbf{M}$. (b) The model of the 3D target.

How to Estimate Matrix A? (The rigid transformation between the tracker and the markers attached to the camera case) Following the previous subsection, we are able to accurately track the set of markers attached to the camera with the C-Track and estimate the transformation matrix $\mathbf{A}$. This matrix is directly available from the tracker.

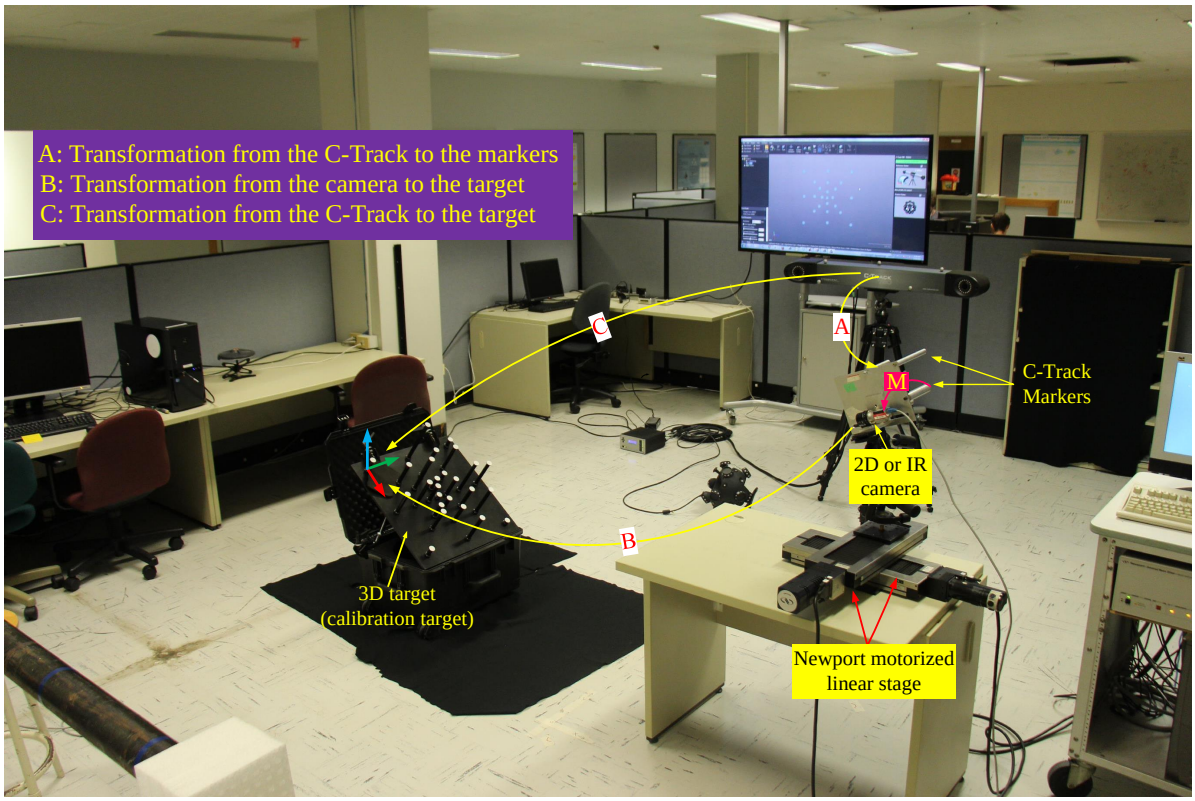

Figure 5: Tracker-Camera (2D/IR) calibration. The setup to calibrate the C-Track with the camera.

How to Estimate Matrix $\mathbf{B} = [\mathbf{R} \mid \mathbf{t}]$? (The rigid transformation between the camera and the 3D target) Assuming that the intrinsic parameters of the 2D (or IR) camera are available and given an image of the 3D target captured by the 2D (or IR) camera, the extrinsic parameters $\mathbf{R}$ and $\mathbf{t}$ in equation (2) can be estimated by detecting the white circular target points at the top of the posts in the image and solving the non-linear optimization problem as proposed in (Zhang, 1999). The accuracy of the calibration matrix $\mathbf{M}$ is highly dependent on the precision of ellipse estimation technique. So, we use a recent approach proposed in (Ouellet and Hébert, 2009) to accurately estimate the parameters of ellipses. The method is based on a linear operator which estimates the parameters in the dual space. So, the procedure of extracting the contour points is eliminated as the raw gradient information of the boundary of ellipses is directly extracted.

How to Estimate Matrix C? (The rigid transformation between the tracker and the 3D target) In order to estimate matrix $\mathbf{C}$, we propose to define a 3D coordinate frame on the target shown in figure 6. This coordinate frame is defined with respect to the C-Track coordinate system and is generated as following:

STEP 1 Scan the surface of three corner posts (i.e. number 1, 3 and 23 in figure 6 (b)) with the MetraSCAN scanner (see figure 7 (a)).

STEP 2 Fit a plane on each surface and then find the best fitting circle to the 3D points lying on the plane with a 25 mm radius which is the size of the disks provided in the calibration file of the 3D target (see figure 7 (a)).

STEP 3 The calibration file of the 3D target provides the coordinates of the top surface of the posts. The center of the fitted circles are projected on the base plane of the 3D target along the normal direction of the corresponding plane with respect to the length of posts which is different for each post (see figure 7 (a)).

STEP 4 Define a plane using the three projected centers (see figure 7 (a)). We will consider the normal of this plane as the Z axis.

STEP 5 Define the axis X using the projected circle

centers 1 and 3.

STEP 6 Compute the axis $Y = Z \times X$, where $\times$ indicates the cross product.

STEP 7 Set the origin at the projected circle center 1 (see figure 7 (b)).

By scanning the top surface of all posts and finding the best fitted circles to the 3D points of each surface (as explained in STEP 2), we can compute the coordinates of each center with respect to the coordinate frame of the 3D target. A comparison between these coordinates and the calibration file of the 3D target will give an estimation of the level of accuracy of the new defined coordinate frame. We achieved $[0.3, 0.5]$ mm as the sum of absolute deviation during several experiments.

It should be mentioned that the resolution of the MetraSCAN scanner is set to 0.2 mm in order to achieve precise fitting results.

Estimation of the Calibration Matrix **M**

As illustrated in figure 5, the calibration matrix **M** can be obtained by closing the loop $\mathbf{AMB} = \mathbf{C}$.
So, $\mathbf{M} = \mathbf{A}^{-1}\mathbf{C}\mathbf{B}^{-1}$.

4 Experimental Results

In this section, experimental results are presented so as to validate the proposed approach and methodology for modeling elongated structures. We use a Basler acA2040-180kc 2D camera with 4MP resolution (Basler, 2016). A Kowa C-mount lens with a fixed focal length of 25 mm and an iris range of F1.4-F16 is used as this 1" lens is suitable for high resolution sensors. We can manually block the iris and the focus with the thumb screws embedded in the lens to ensure the reliability of calibration parameters.

To calibrate the intrinsic parameters we use the approach proposed in (Zhang, 1999) and the 2D planar target with $16 \times 16 = 256$ circular markers in figure 3. In the numerous experiments that were conducted we achieved $[0.095, 0.100]$ pixel as reprojection error for 10 to 16 images captured from different positions and orientations. In practice, the reprojection error was constant with 4 digits precision for more than 10 images.

The tracking model of the camera is built with 11 retro-reflective markers as illustrated in figure 4. The procedure of outlier removal using the absolute deviation around the median (MAD) is iteratively performed until a 1 µm difference to the sum of absolute deviation (SAD) was reached. Moreover, applying the ICP refinement on the pose of the tracking model

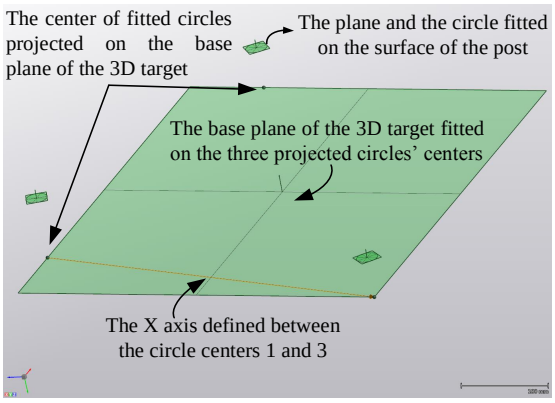

(a)

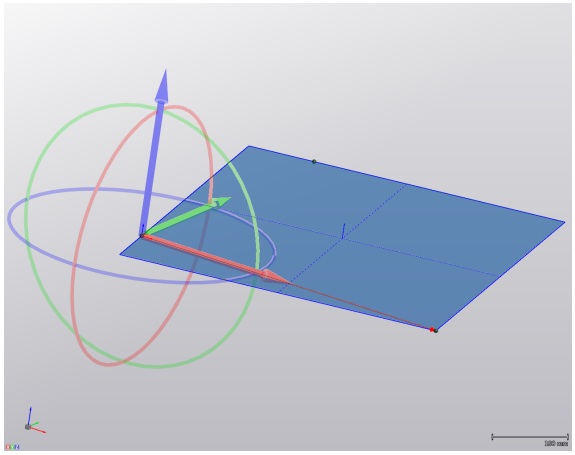

(b)

Figure 7: Construction of a 3D coordinate frame on the 3D target with respect to the C-Track coordinate system. (a) The entities used to define the 3D coordinate frame (b) The defined 3D coordinate frame with respect to the C-Track coordinate system.

provides an improvement of 0.233 mm on the pose estimation.

The calibration matrix **M** is computed using the 3D target presented in figure 6 and the calibration procedure proposed in Section 3.2.2. We evaluate the accuracy of the calibration matrix based on the *reprojection error* which is computed using the following steps:

1) Capture an image of the 3D target.
2) Track the pose of the camera to estimate the rigid transformation between the C-Track and the markers attached to the camera case (matrix **A** in figure 5).
3) Scan the surface of the posts that are visible in the image with the MetraSCAN scanner.

4) Fit a plane to each surface of the scan (i.e. the planar top of the posts) and then find the best fitting circle to the 3D points lying on the plane with a 25 mm radius which is the size of the disks as provided in the calibration file of the 3D target.

5) Project the fitted circles on the image using matrices **A**, **M** and **K** according to equation (2) (see figure 8).

6) Compute the reprojection error as the mean absolute deviation of the projected center of circles and the center of ellipses detected in the image. The error computed above is expressed in pixel units which can be converted into mm based on the focal length and the distance of the 3D target from the camera in the direction of the optical axis according to the pinhole model.

Since we use the same data sets that were used to compute matrix **M**, we expect to obtain a reprojection error close to zero mm (or pixel). As observed in figure 8 (a) a mean absolute deviation of 1.04 pixel that is equivalent to 0.56 mm is estimated.

The reprojection error increases if the camera moves due to the additional error resulting from pose tracking. Figure 8 (b) presents the reprojection error for a second pose of the camera. The mean absolute deviation of the computed error is 1.69 pixels which is equivalent to 0.9 mm. In practice, the reprojection error for calibration matrix **M** was less than 1.5 mm for the experiments.

A related point to consider is the procedure of data collection. Since, the range of view of the photogrammetric system is limited to collect data along the large structure, the tracking system has to be moved in a leapfrog manner (see ïňĄgure 1) as proposed in (Hesabi and Laurendeau, 2016). It means that multiple 3D data sets captured from different view points must be registered in order to cover the full structure. The accumulation error caused by this leapfrog strategy has absolutely an impact on mapping results but with a constant value. In order to estimate this effect, we performed an experiment with one leapfrog movement of the C-Track (meaning two positions of the C-Track in the scene) and three positions of the 2D camera for the set of the two leapfrog positions. The result of mapping RGB images on 3D data is presented in figure 9. The left and middle images are taken at the first pose of the C-Track, so the 0.2 mm error which is visible in the misaligned letters "rt" (comparing figure 9 (d) and (e)) indicates the mapping error of one pose of the C-Track. The misaligned letters "ew" in figure 9 (g) compared to (f) represent two accumulative errors: the mapping error and the registration error of the leapfrog movement. So, the error increases to

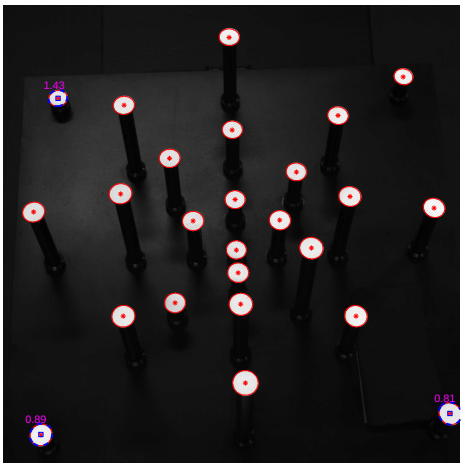

(a)

(b)

Figure 8: The reprojection error of the calibration matrix **M** using the data acquired to estimate it. The ellipses detected in the image are presented in red. The circles fitted to the 3D points acquired from the surface of posts are projected on the image which are illustrated in blue for these posts with floating magenta numbers. The error is measured in pixels where one pixel is equal to 0.5 mm.

0.45 mm.
It should be highlighted that, in spite of the unavoidable error caused by the leapfrog strategy, the proposed procedure for modeling elongated structures provides sub-millimeter accuracy.

To further illustrate the reliability of our modeling methodology, we performed an experiment with six sets of data points acquired from a pipeline model which contains T-junctions, corners and sleeves. The

(a)

(b)

(c)

(d)

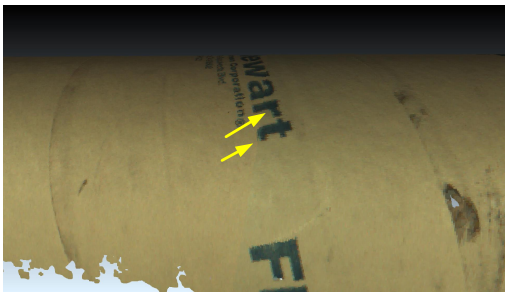

(e)

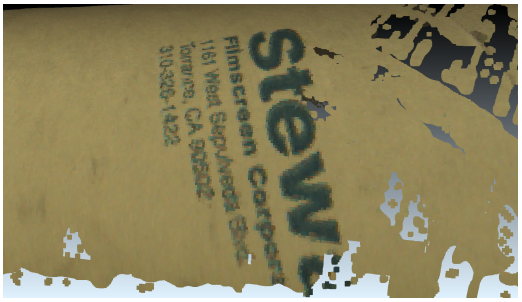

(f)

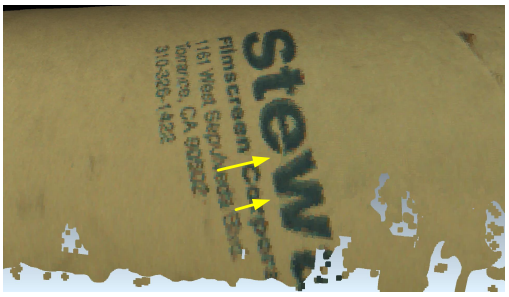

(g)

Figure 9: Mapping RGB images on 3D data acquired by one leapfrog movement of the C-Track. (a) The 3D data of the surface of a cylinder acquired by the MetraSCAN scanner with 0.2 mm resolution and aligned as proposed in (Hesabi and Laurendeau, 2016). Different colors represent different meshes. (b) Three RGB images taken from the surface of the cylinder are presented in different colors. (c) The result of mapping RGB images on 3D data. (d)-(e) The 0.2 mm error is visible in the misaligned letters "rt". (f)-(g) A larger error, 0.45 mm, due to the leapfrog movement caused a visible misalignment in the letters "ew" (the area of this error, which is very small and difficult to see is pointed to by the yellow arrow).

overall accuracy of the proposed methodology for this pipeline is compared to ground truth data, which was provided by a LiDAR (Light Detection And Ranging) sensor (Trimble® TX5 3D laser scanner) (Trimble, 2016) with an accuracy of 2 mm standard deviation for its 3D measurements. The comparison is performed using InnovMetric's PolyWorks® commercial 3D inspection software[1], with the IMInspect module (InnovMetric, 2016). According to this comparison, our 3D modeling methodology is reliable with a precision of 99.957% of points within $\pm 3\times$standard deviations for a standard deviation of 0.992 mm. This level of reliability emphasizes that our proposed approach is able to build an accurate 3D model of pipelines or other similar elongated structures in an inspection context where the objective is to assess the evolution of defects at different time intervals.

Moreover, the repeatability of the proposed mapping procedure was investigated according to the following repeatability conditions (ISO, 2016):

- the same measurement procedure,
- the same operator,
- the same measuring equipment used under the same conditions,
- the same location,
- repetition over a short period of time.

Considering the repeatability of the C-Track which is up to 0.0025 mm (Creaform, 2016), we performed 16 experiments following the proposed approach. Table 3.4 illustrates the reprojection error of the calibration matrix **M**. Considering the standard deviation of the reprojection errors of the calibration matrix **M**, the repeatability measurement is 44 µm which indicates the mapping procedure is highly repeatable. This means that in an inspection context, one can assess the evolution of defects by comparing the reconstructed models at different times and be confident of the assessment.

Table 1: The result of 16 experiments to estimate the reprojection error of the calibration matrix **M**

Experiment number	Reprojection error
1	0.478 mm
2	0.451 mm
3	0.537 mm
4	0.531 mm
5	0.532 mm
6	0.542 mm
7	0.572 mm
8	0.574 mm
9	0.582 mm
10	0.508 mm
11	0.537 mm
12	0.464 mm
13	0.531 mm
14	0.587 mm
15	0.576 mm
16	0.477 mm

5 CONCLUSIONS

In this paper, we presented a repeatable and simple procedure to accurately map RGB or IR information on the 3D data in the context of inspection of very elongated structures such as but not limited to pipelines. A metrologic handheld 3D scanner is used to build the geometric model of the elongated structure of interest. As each sensor acquires the information in its own local reference frame, we proposed a precise and repeatable calibration procedure which enables us to combine the 3D data with IR information. The results indicate that the proposed method is efficient, accurate and highly repeatable for the tasks such as inspection of pipelines and can be used for applications in metrology.

[1]Polyworks® is a widely used inspection tool for quality control and inspection in industry.

ACKNOWLEDGEMENTS

This research was supported by the NSERC-Creaform industrial research chair on 3D scanning.

REFERENCES

Basler (2016). Basler, the power of sight. `http://www.baslerweb.com/en/products/cameras/area-scan-cameras/ace/aca2040-180kc`.

Bauer, M., Schlegel, M., Pustka, D., Navab, N., and Klinker, G. (2006). Predicting and estimating the accuracy of n-occular optical tracking systems. In *2006 IEEE/ACM International Symposium on Mixed and Augmented Reality*, pages 43–51. IEEE.

Besl, P. J. and McKay, N. D. (1992). Method for registration of 3-d shapes. In *Robotics-DL tentative*, pages 586–606. International Society for Optics and Photonics.

Creaform (2016). Dynamic tracking-vxtrack. http://www.creaform3d.com/en/metrology-solutions/3d-applications-software-platforms/dynamic-tracking-vxtrack.

Fitzpatrick, J. M., West, J. B., and Maurer, C. (1998). Predicting error in rigid-body point-based registration. *IEEE transactions on medical imaging*, 17(5):694–702.

Hesabi, S. and Laurendeau, D. (2016). Aligning 3d local data of leapfrog locations along elongated structures. In *Computer and Robot Vision, 2016. CRV '2016. 13th Canadian Conference on*. IEEE Computer Society.

InnovMetric (2016). Innovmetric software | your 3D metrology software partner. http://www.innovmetric.com/.

ISO, D. (2016). 5725-1: 1994. *Accuracy (trueness and precision) of Measurement Methods and Results-Part 1: General Prinicples and Definitions*.

Levinson, J. and Thrun, S. (2013). Automatic online calibration of cameras and lasers. In *Robotics: Science and Systems*, pages 24–28.

Leys, C., Ley, C., Klein, O., Bernard, P., and Licata, L. (2013). Detecting outliers: Do not use standard deviation around the mean, use absolute deviation around the median. *Journal of Experimental Social Psychology*, 49(4):764–766.

Napier, A., Corke, P., and Newman, P. (2013). Cross-calibration of push-broom 2d lidars and cameras in natural scenes. In *Robotics and Automation (ICRA), 2013 IEEE International Conference on*, pages 3679–3684. IEEE.

Ouellet, J.-N. (2011). *Ré-observabilité des points caractéristiques pour le calibrage et le positionnement d'un capteur multi-caméra*. PhD thesis, Université Laval.

Ouellet, J.-N. and Hébert, P. (2009). Precise ellipse estimation without contour point extraction. *Machine Vision and Applications*, 21(1):59–67.

Pandey, G., McBride, J. R., Savarese, S., and Eustice, R. M. (2015). Automatic extrinsic calibration of vision and lidar by maximizing mutual information. *Journal of Field Robotics*, 32(5):696–722.

Quan, L. and Lan, Z. (1999). Linear n-point camera pose determination. *IEEE Transactions on pattern analysis and machine intelligence*, 21(8):774–780.

Scaramuzza, D., Harati, A., and Siegwart, R. (2007). Extrinsic self calibration of a camera and a 3d laser range finder from natural scenes. In *2007 IEEE/RSJ International Conference on Intelligent Robots and Systems*, pages 4164–4169. IEEE.

Trimble (2016). Trimble, transforming the way the world works. http://www.trimble.com/.

Unnikrishnan, R. and Hebert, M. (2005). Fast extrinsic calibration of a laser rangefinder to a camera.

Vogt, S., Khamene, A., Sauer, F., and Niemann, H. (2002). Single camera tracking of marker clusters: Multiparameter cluster optimization and experimental verification. In *Proceedings of the 1st International Symposium on Mixed and Augmented Reality*, page 127. IEEE Computer Society.

Wasielewski, S. and Strauss, O. (1995). Calibration of a multi-sensor system laser rangefindercamera. In *Intelligent Vehicles' 95 Symposium., Proceedings of the*, pages 472–477. IEEE.

West, J. B. and Maurer, C. R. (2004). Designing optically tracked instruments for image-guided surgery. *IEEE transactions on medical imaging*, 23(5):533–545.

Woltring, H., Huiskes, R., De Lange, A., and Veldpaus, F. (1985). Finite centroid and helical axis estimation from noisy landmark measurements in the study of human joint kinematics. *Journal of biomechanics*, 18(5):379–389.

Zhang, Z. (1999). Flexible camera calibration by viewing a plane from unknown orientations. In *Computer Vision, 1999. The Proceedings of the Seventh IEEE International Conference on*, volume 1, pages 666–673. IEEE.